Reduction of residual amplitude modulation to 1 × 10⁻⁶ for frequency modulation and laser stabilization

W. Zhang,[1,*] M. J. Martin,[1,4] C. Benko,[1] J. L. Hall,[1] J. Ye,[1] C. Hagemann,[2]
T. Legero,[2] U. Sterr,[2] F. Riehle,[2] G. D. Cole,[3] and M. Aspelmeyer[3]

[1]*JILA, National Institute of Standards and Technology and University of Colorado, Boulder, Colorado 80309-0440, USA*

[2]*Physikalisch-Technische Bundesanstalt (PTB), Bundesallee 100, 38116 Braunschweig, Germany*

[3]*Vienna Center for Quantum Science and Technology (VCQ), Faculty of Physics, University of Vienna, A-1090 Vienna, Austria*

[4]*Currently at Norman Bridge Laboratory of Physics, Caltech, Pasadena, California 91127, USA*

Corresponding author: w.zhang@JILA.colorado.edu

Active control and cancellation of residual amplitude modulation (RAM) in phase modulation of an optical carrier is one of the key technologies for achieving the ultimate stability of a laser locked to an ultrastable optical cavity. Furthermore, such techniques are versatile tools in various frequency modulation-based spectroscopy applications. In this Letter we report a simple and robust approach to actively stabilize RAM in an optical phase modulation process. We employ a waveguide-based electro-optic modulator (EOM) to provide phase modulation and implement an active servo with both DC electric field and temperature feedback onto the EOM to cancel both the in-phase and quadrature components of the RAM. This technique allows RAM control on the parts-per-million level where RAM-induced frequency instability is comparable to or lower than the fundamental thermal noise limit of the best available optical cavities. © 2014 Optical Society of America

Frequency modulation techniques are widely utilized in fields employing precision control of lasers, such as laser spectroscopy [1,2] and gravitational wave detection [3–5], and for cavity-based laser frequency stabilization [6–13]. However, frequency or phase modulation processes are often degraded by residual amplitude modulation (RAM) that arises when the modulation sidebands are unequal in magnitude, not exactly opposite in phase, or both. Fluctuating RAM thus appears as an unwanted noise around the modulation frequency, imposing a limitation on the fidelity of signal recovery. For cavity-based laser stabilization using the Pound–Drever–Hall (PDH) radio frequency (RF) sideband technique, RAM introduces frequency offset noise to the servo error signal and thus degrades the laser frequency stability. RAM also limits the accuracy for the determination of the unperturbed line center [2].

A variety of effects can give rise to RAM [14,15]. For example, optical scattering and parasitic interferences between any parallel surfaces (etalons) along the optical beam path can induce RAM. Compounding matters, these effects are often sensitive to temperature variations and mechanical vibrations, impeding the realization of field deployed stabilized laser systems [11]. An electro-optic modulator (EOM) is an essential component to provide optical phase modulation; however, this device is in many cases the main source of RAM if parasitic optical effects are not eliminated. When the polarization of the input beam is misaligned with one of the principal axes of the electro-optic crystal, each polarization component experiences different phase shifts, which can fluctuate under temperature and stress-dependent birefringence variations of the modulator crystal. Polarizing optical components downstream will thus convert this polarization/phase noise into RAM. One might expect that, for a free-space bulk crystal, it is possible to reduce the polarization-rotation-induced RAM with extreme care in aligning the polarization of the optical field to match the crystal's principal axes. However, for precision control applications, it is challenging to sufficiently suppress and stabilize RAM with this passive method due to the instabilities in alignment induced by temperature fluctuations and mechanical vibrations, spatial inhomogeneity of the electric field inside the crystal, or scattering and etalon effects arising from crystal defects or backreflections from imperfect antireflection coatings. As a result, these crystal-related effects are the dominant contribution to the overall RAM of the system.

Several methods have been implemented to suppress RAM [14–20]. Briefly, RAM arising from polarization rotation is the amplitude at the modulation frequency ω_m for the photo-current I [14],

$$I(\omega_m) = -\sin(2\beta)\sin(2\gamma)|\epsilon_0|^2 J_1(M)$$
$$\times \sin(\omega_m t)\sin(\Delta\phi + \Delta\phi^{\mathrm{DC}}). \quad (1)$$

Here, $\sin(2\beta)$ and $\sin(2\gamma)$ are polarization alignment factors [14] that are sensitive to vibration and temperature; ϵ_0 is the amplitude of the optical field; $J_1(M)$ is the first order Bessel function with M being the difference of the modulation indices of the ordinary and extraordinary polarizations; $\Delta\phi$ is the phase shift due to natural birefringence that is temperature and stress dependent; and $\Delta\phi^{\mathrm{DC}}$ is the compensating phase shift due to a DC electric field applied to the crystal. From Eq. (1), we realize that when $\sin(\Delta\phi + \Delta\phi^{\mathrm{DC}}) = 0$, that is, the effect of the phase shift due to natural birefringence is compensated by the phase shift due to the applied DC field, the overall EOM-related RAM can be suppressed to a

high degree. This is the core of the method we employ for the active RAM stabilization shown in this Letter.

Control of RAM to the highest possible degree is always desirable, but it is particularly true for the development of cavity-stabilized laser systems. By using a long cavity spacer [13] or employing crystalline materials with low thermal noise [11,21], the state-of-the-art laser frequency stability has reached the 10^{-16} level, limited nearly exclusively by the reference cavity thermal noise. To reach the 10^{-17} stability level, which is now feasible with the reduced thermal noise enabled by advanced reference cavity technologies, RAM-induced frequency noise must be further suppressed. Meanwhile, portable cavity systems [22,23] require a compact design, where a given RAM magnitude will induce larger fractional frequency noise due to the reduced cavity length. Here, we employ a waveguide-based EOM (Ti-diffused waveguide in $LiNbO_3$) to provide phase modulation for a cavity-stabilized laser system and describe an active servo loop involving both DC electric field and temperature corrections applied to the EOM. The DC electric field affects the in-phase response 20 times larger than the quadrature response. In contrast, the in-phase response of the temperature control is 0.2 times that of the quadrature response. Working in tandem, the two transducers suppress both the in-phase and quadrature components of the RAM to the 1 parts-per-million (ppm) level over an extended time. The removal of the long-term drift of RAM represents a key improvement over previous results [15,18].

The waveguide-based EOM is integrated with polarization-maintaining (PM) fibers for the input and output optical fields. This configuration has intrinsic advantages when compared with a free-space bulk crystal. First, to produce a similar optical phase shift, the values of a modulation voltage applied to the waveguide-based EOM are 2 orders of magnitude lower than that for a bulk crystal. For example, the voltage to achieve a π phase shift is approximately 4 V for a waveguide EOM, while it is typically above 100 V for a free-space bulk crystal even when its dimensions are optimized for low π voltage. Such a reduction in the required voltage eases the control requirements. Second, the input fiber acts as an effective spatial mode cleaner, providing a small input beam size to the crystal, reducing RAM contributions arising from the spatial inhomogeneity of the optical field interacting with spatially varying index profile of the crystal that is driven by the RF field. Third, the output fiber provides a high-quality quasi-TEM_{00} mode for the subsequent optical components, thus producing a uniform optical wavefront with negligible spatial inhomogeneity encoded on the RAM. The spatial homogeneity of the modulated output is critical for the RAM servo. In such a configuration, the photodetector sees only the spatially averaged RAM, which is then corrected to zero by the servo. A nonuniform RAM distribution entails that a subsequent photodetector used for the PDH error signal generation would detect its own spatially averaged RAM that is different from that of the servo detector. Fourth, the integrated structure of the waveguide EOM stabilizes the beam position on the crystal, thus preventing variation of the RAM phase due to deviations in the beam position. Although it is inevitable to have a small
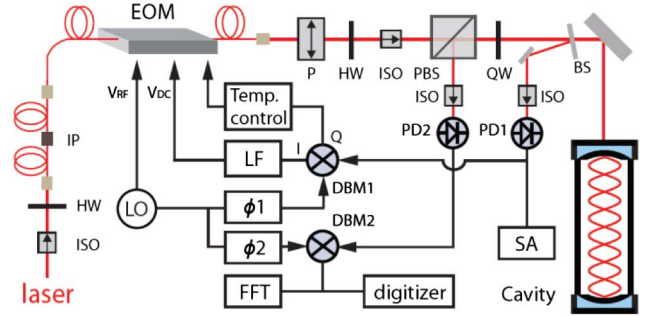

Fig. 1. Experimental scheme for active RAM stabilization. After passing through the phase modulator, a portion of the light is detected by PD1 for active RAM control, and PD2 is used for PDH signal and out-of-loop RAM measurement. EOM, waveguide-based electro-optic modulator; V_{RF}, RF signal for phase modulation; V_{DC}, direct current field applied to EOM for active RAM cancellation; IP, in-line polarizer; P, free-space polarizer; BS, beam splitter; PBS, polarization beam splitter; HW, half-wave plate; QW, quarter-wave plate; ISO, optical isolator; PD, photodetector; DBM, double-balanced mixer; I(Q) mixer in-phase (quadrature) port; φ, phase shifter; SA, spectrum analyzer; LO local oscillator (10.5 MHz); LF, loop filter; FFT, fast Fourier transform (FFT) analyzer.

misalignment between the principal axes of the waveguide EOM and the axis of the fibers, the corresponding RAM noise due to the vibrations and temperature fluctuations of the fiber can be compensated with $\Delta\phi^{DC}$.

Figure 1 illustrates the experimental setup used for cavity stabilization of the laser frequency, including the PDH locking configuration and the active RAM servo. Here, we demonstrate an active RAM servo for a short-length (35 mm) optical cavity employing crystalline coating end mirrors [21]. The cavity finesse is 150,000 at wavelength of 1.064 μm, yielding a FWHM of 28 kHz. A continuous wave laser from an all solid-state, diode-pumped nonplanar ring oscillator is used for this work. An optical isolator in front of the laser is used to minimize backreflections. A PM fiber mating sleeve is used to connect the in-line polarizer and the waveguide EOM. To sufficiently suppress scattering and spurious etalon effects in the optical setup, all optical surfaces are tilted slightly off of normal incidence for the laser beam, and additional optical isolators are placed in front of the polarization beam splitter and photodetectors.

The PDH error signal is used to lock the laser to a cavity resonance. When the laser frequency is tuned far from the cavity resonance, fluctuations of the PDH error signal recovered with PD2 represent the out-of-loop RAM of the entire system. To continuously measure RAM, an optical beam splitter is placed close to the cavity input with a small angle of incidence so as to detect RAM that is nearly identical to that seen by the cavity. To monitor the amplitude of the RAM, a directional coupler follows the photodetector (PD1) and the −20 dB output is fed to an RF spectrum analyzer. The same RF signal used for frequency modulation acts as a local oscillator to be mixed with the RAM detector signal. The phase of the local oscillator is adjusted to give a maximum RAM signal in the mixer output. The RAM error signal is processed with a loop filter that controls the DC electric field applied to the EOM. This actively cancels the in-phase
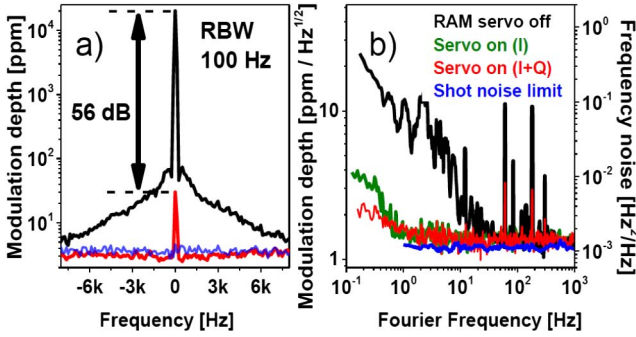
Fig. 2.   (a) RAM reduction realized with the active cancellation scheme. The power spectrum of the in-loop RAM signal received by PD1 is recorded on a spectrum analyzer with 100 Hz resolution bandwidth. The RAM signal with active servo on (red line) is 56 dB lower than that without servo (black line). Blue line, shot noise floor. This remaining RAM is stable at the 3% level. (b) Left axis: power spectral density (PSD) of the out-of-loop RAM fluctuations, i.e., off-resonant PDH signal obtained from PD2. The noise corresponding to RAM with active cancellation (red and green lines) is approximately 20 times lower than the result without servo (black line) at 1 Hz. At low Fourier frequencies, simultaneous in-phase and quadrature servos (red line) achieve better stability than that with only in-phase servo (green line). The noise floor (blue line) is set by the shot noise of PD2. Right axis: corresponding PSD of the frequency noise for the cavity-stabilized 1.064 μm laser. The voltage noise is converted to frequency noise by the slope of the cavity frequency discrimination.

RAM of the EOM, as illustrated with Eq. (1). The servo bandwidth is typically 200 kHz. It is not surprising that there are additional mechanisms, such as the spatial non-uniformity of the modulated wavefront and beam steering arising from the piezoelectric-induced elasto-optic effect of the EOM. This can give rise to a quadrature component for the RAM [18]. To suppress this component, the output of the mixer quadrature port is fed to a slow integrator that produces a feedback to the EOM temperature. The bandwidth of the quadrature RAM servo is smaller than 0.1 Hz, which is limited by the EOM thermal response time. The gain of this servo is adjusted to avoid cross talk with the in-phase RAM servo since the thermal control does not purely affect the quadrature RAM.

Figure 2(a) shows the amplitude of the in-loop RAM in units of modulation depth monitored by PD1 and recorded with the spectrum analyzer. When the in-phase and quadrature RAM servos are activated simultaneously, the RAM is suppressed by 56 dB. The remaining but stable RAM achieved is approximately 20 dB higher than the shot noise floor of PD1 (0.25 mA photocurrent) at a resolution bandwidth of 100 Hz. As the residual RF pickup is 20 dB below this signal, we suspect that the stable 30 ppm RAM comes from residual etalon effects in the optical setup. This remaining RAM shows excellent stability at the percent level.

For cavity-stabilized laser applications, it is important to evaluate the RAM-induced fractional frequency instability. To further investigate the noise components of the remaining RAM, the noise power spectral density (PSD) of the out-of-loop RAM signal, that is, the off-resonant PDH error signal recovered with PD2, is measured with a fast Fourier transform (FFT) analyzer. At 1 Hz the PSD

of the stabilized RAM is approximately 20 times lower than the free-running result. Furthermore, at low Fourier frequencies, the quadrature RAM servo provides an effective long-term stabilization. At high Fourier frequencies beyond 10 Hz, the detection is limited by the shot noise of PD2. The shot noise of PD1 used in the servo makes a negligible contribution (~10%) to the out-of-loop noise. To quantify the relation between RAM fluctuation and frequency noise, the corresponding frequency noise PSD is plotted along the right vertical axis in Fig. 2(b). The laser linewidth due to the stabilized RAM is ≪1 Hz.

To demonstrate the long-term stability of the stabilized RAM, Fig. 3(a) shows a time record of the out-of-loop RAM signal from PD2 recorded by a digitizer and displayed as modulation depth in units of ppm. By using the in-phase and quadrature servos, the peak-to-peak RAM fluctuation is maintained within ±5 ppm for more than 2 h, without noticeable drift. Furthermore, as shown in Fig. 3(b), the Allan deviation associated with the RAM fluctuation, σ_{RAM}, is at the 1 ppm level for averaging times τ from 1 to 1000 s, indicating 3% stability relevant to the remaining value of the RAM. Since σ_{RAM} is determined from the off-resonance PDH signal, when the laser is locked on cavity resonance, the RAM-induced fractional frequency instability, σ_y, is estimated to have an upper bound of

$$\sigma_y = \sigma_{\mathrm{RAM}} \times \frac{\kappa}{\nu}. \tag{2}$$

Here, κ is cavity linewidth and ν is optical carrier frequency. According to Eq. (2), for the 35 mm cavity with $\kappa = 28$ kHz at 1.064 μm, σ_{RAM} at 1 ppm would correspond
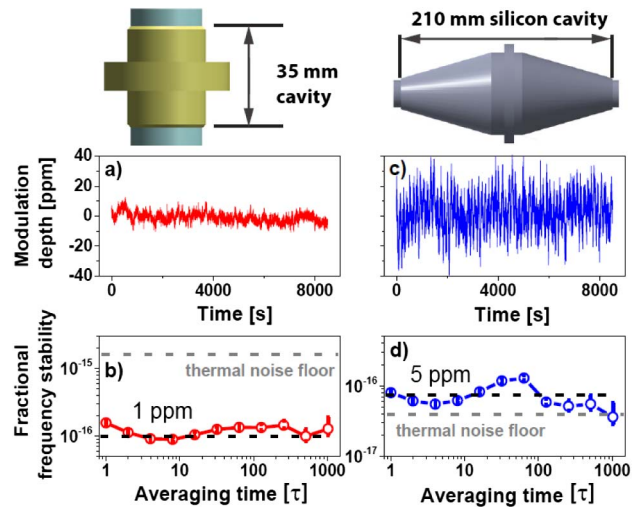

Fig. 3.   Out-of-loop RAM signal recorded with PD2 when the laser is detuned far off the cavity resonance. The linewidth of the 35 mm cavity is 28 kHz at a wavelength of 1.064 μm. The silicon cavity is 210 mm in length, resulting in a significantly reduced cavity linewidth of 3 kHz at 1.5 μm. (a) and (c) The modulation depth of the stabilized RAM based on the 35 mm cavity and the 210 mm silicon cavity, respectively. (b) and (d) RAM-induced fractional frequency instability corresponding to the data in (a) and (c), respectively. The black-dashed lines indicate the fractional frequency instability corresponding to 1 and 5 ppm RAM fluctuations, respectively, and the gray-dashed line is thermal-noise-limited frequency stability for each cavity.

to σ_y of 1×10^{-16}. We note that the thermal-noise-limited fractional frequency instability of the 35 mm cavity is 1×10^{-15} for averaging times of 1–1000 s [21]; thus, the contribution of the stabilized RAM to the total frequency instability is negligible. On the other hand, when the RAM servo is off, the resulting frequency instability exceeds 1×10^{-15} at 1 s and increases with time at a slope of approximately $\sqrt{\tau}$ due to the uncontrolled drift. This is directly confirmed in an optical heterodyne beat experiment between this system and the Sr local oscillator [13] via an Yb:fiber frequency comb [24].

We also successfully implement the active RAM servo on another cavity-stabilized laser system, this time based on a single-crystal silicon cavity [11] with a length of 210 mm and a linewidth of 3 kHz at wavelength of 1.5 μm. Here, in a similar fashion, we activate the in-phase RAM servo by providing a DC electric field to the EOM. The peak-to-peak fluctuation of the stabilized RAM shown in Fig. 3(c) is on the ±25 ppm level. The corresponding Allan deviation [Fig. 3(d)] reveals that the RAM is stabilized at the 5 ppm level from 1 to 1000 s, resulting in a RAM-limited frequency instability of 8×10^{-17}, which is close to the silicon cavity thermal noise limit. Again, compared to the free-running case, the active RAM servo provides at least 1 order of magnitude improvement for frequency stability. Obviously, a longer cavity length is advantageous for improved frequency stability for a given RAM magnitude, similar to the case for thermal noise.

In conclusion, we have achieved RAM stabilization at the 1×10^{-6} level by using an active servo comprising in-phase and quadrature RAM corrections, limited by shot noise at Fourier frequencies beyond 10 Hz. This rigorous RAM control method, which should be applicable to various EOMs, allows for frequency stabilization comparable to the fundamental thermal noise limit of the best available optical cavities, approaching the 10^{-17} level. Better long-term stability can be achieved by improving optical isolation in order to reduce residual etalon effects in the optical path. Higher finesse mirrors supporting narrower cavity linewidth are also beneficial for reducing the RAM-induced frequency instability.

References

1. G. C. Bjorklund, Opt. Lett. **5**, 15 (1980).
2. J. Ye, L.-S. Ma, and J. L. Hall, J. Opt. Soc. Am. B **15**, 6 (1998).
3. LIGO Scientific Collaboration, Rep. Prog. Phys. **72**, 076901 (2009).
4. S. Barke, M. Tröbs, B. Sheard, G. Heinzel, and K. Danzmann, Appl. Phys. B **98**, 33 (2010).
5. K. Kokeyama, K. Izumi, W. Z. Korth, N. Smith-Lefebvre, K. Arai, and R. X. Adhikari, J. Opt. Soc. Am. A **31**, 81 (2014).
6. R. W. P. Drever, J. L. Hall, F. V. Kowalski, J. Hough, G. M. Ford, A. J. Munley, and H. Ward, Appl. Phys. B **31**, 97 (1983).
7. B. C. Young, F. C. Cruz, W. M. Itano, and J. C. Bergquist, Phys. Rev. Lett. **82**, 3799 (1999).
8. H. Stoehr, F. Mensing, J. Helmcke, and U. Sterr, Opt. Lett. **31**, 736 (2006).
9. A. D. Ludlow, X. Huang, X. M. Notcutt, T. Zanon-Willette, S. M. Foreman, M. M. Boyd, S. Blatt, and J. Ye, Opt. Lett. **32**, 641 (2007).
10. J. Alnis, A. Matveev, N. Kolachevsky, T. Udem, and T. W. Hänsch, Phys. Rev. A **77**, 053809 (2008).
11. T. Kessler, C. Hagemann, C. Grebing, T. Legero, U. Sterr, F. Riehle, M. J. Martin, L. Chen, and J. Ye, Nat. Photonics **6**, 687 (2012).
12. T. L. Nicholson, M. J. Martin, J. R. Williams, B. J. Bloom, M. Bishof, M. D. Swallows, S. L. Campbell, and J. Ye, Phys. Rev. Lett. **109**, 230801 (2012).
13. M. J. Martin, M. Bishof, M. D. Swallows, X. Zhang, C. Benko, J. von-Stecher, A. V. Gorshkov, A. M. Rey, and J. Ye, Science **341**, 632 (2013).
14. N. C. Wong and J. L. Hall, J. Opt. Soc. Am. B **2**, 1527 (1985).
15. L. Li, F. Liu, C. Wang, and L. Chen, Rev. Sci. Instrum. **83**, 043111 (2012).
16. A. Whittaker, C. M. Shum, H. Grebel, and H. Lotem, J. Opt. Soc. Am. B **5**, 1253 (1988).
17. S. Kasapi, S. Lathi, and Y. Yamamoto, J. Opt. Soc. Am. B **17**, 275 (2000).
18. C. Ishibashi, J. Ye, and J. L. Hall, in *Quantum Electronics and Laser Science Conference*, Long Beach, California, May 19–24 (IEEE, 2002), paper QTuF27.
19. H. Müller, S. Herrmann, T. Schuldt, M. Scholz, E. Kovalchuk, and A. Peters, Opt. Lett. **28**, 2186 (2003).
20. F. Du Burck, O. Lopez, and A. El Basri, IEEE Trans. Instrum. Meas. **52**, 288 (2003).
21. G. D. Cole, W. Zhang, M. J. Martin, J. Ye, and M. Aspelmeyer, Nat. Photonics **7**, 644 (2013).
22. D. R. Leibrandt, M. J. Thorpe, J. C. Bergquist, and T. Rosenband, Opt. Express **19**, 10278 (2011).
23. B. Argence, E. Prevost, T. Lévèque, R. Le Goff, S. Bize, P. Lemonde, and G. Santarelli, Opt. Express **20**, 25409 (2012).
24. C. Benko, A. Ruehl, M. J. Martin, K. S. E. Eikema, M. E. Fermann, I. Hartl, and J. Ye, Opt. Lett. **37**, 2196 (2012).